Urban Climate 31 (2020) 100565

Contents lists available at ScienceDirect

Urban Climate

journal homepage: www.elsevier.com/locate/uclim

The urban climate of Ghent, Belgium: A case study combining a high-accuracy monitoring network with numerical simulations

Steven Caluwaerts[a,*], Rafiq Hamdi[a,b], Sara Top[a], Dirk Lauwaet[c], Julie Berckmans[b,c,d], Daan Degrauwe[a,b], Herwig Dejonghe[a], Koen De Ridder[c], Rozemien De Troch[a,b], Francois Duchêne[b], Bino Maiheu[c], Michiel Van Ginderachter[a,b], Marie-Leen Verdonck[e], Thomas Vergauwen[a], Guy Wauters[a], Piet Termonia[a,b]

[a] Department of Physics and Astronomy, Ghent University, Krijgslaan 281, 9000 Gent, Belgium
[b] Royal Meteorological Institute, Brussels, Belgium
[c] VITO, Mol, Belgium
[d] Centre of Excellence PLECO (Plants and Ecosystems), University of Antwerp, Belgium
[e] FORSIT, Ghent University, Belgium

ARTICLE INFO

Keywords:
High-resolution urban modelling
Urban heat island
Urban monitoring network
ALARO-0
SURFEX
UrbClim

ABSTRACT

As urban environments have a specific climate that poses extra challenges (e.g. increased heat stress during heat waves), gaining detailed insight into the urban climate is important. This paper presents the high-accuracy MOCCA (MOnitoring the City's Climate and Atmosphere) network, which is monitoring the urban climate of the city of Ghent since July 2016. The study illustrates the complementarity between modelling and observing the urban climate. Two different modelling approaches are used: 1 km resolution runs of the SURFEX land surface model and 100 m resolution runs of the computationally cheaper UrbClim boundary layer model. On the one hand, urban models are able to simulate the spatial variability of the urban climate. As such, these models serve as a tool to help deciding on the locations of the measurement stations. On the other hand, the MOCCA observations are used to validate the high-resolution urban model experiments for the summer (July-August-September) of 2016. Our results demonstrate that the models capture the nighttime intra-urban temperature differences, but they are not able to reproduce the observed daytime temperature differences which are determined by the micro-scale environment.

1. Introduction

As the world is urbanizing at a high rate, urban meteorology is gaining interest and importance. The elevated temperature in the city, known as the urban heat island (UHI), is the best documented illustration of human climate modifications. The physical basis of the UHI is extensively discussed in literature e.g. Arnfield (2003). The interaction between the city and the atmosphere involves different spatial scales. Measurements in the urban canopy layer (UCL), which is roughly defined as the layer of air below the rooftops, are strongly determined by microscale features, implying that a representative siting is necessary in order to have meaningful UCL observations. Above roof level, in the so-called urban boundary layer (UBL), the larger scale urban properties start to dominate. Urban monitoring networks can be classified according to the scale they study (Muller et al., 2013). The MOCCA

* Corresponding author.
E-mail address: steven.caluwaerts@ugent.be (S. Caluwaerts).

https://doi.org/10.1016/j.uclim.2019.100565
Received 25 April 2019; Received in revised form 12 September 2019; Accepted 11 November 2019

(MOnitoring the City's Climate and Atmosphere) network presented in this paper is a city-scale network designed to monitor the canopy layer UHI.

To gain insight into the urban climate two complementary approaches are used: modelling studies and observational campaigns. High resolution atmospheric modelling of cities all over the world is carried out to investigate UHIs under current and future climate conditions and to study mitigation measures. Reliable urban meteorological data are needed to validate the urban model outcomes. There exists an extensive body of literature presenting observational urban data but by studying a large sample of UHI studies Stewart (2011) concluded that nearly half of them are scientifically indefensible. Therefore, there is still an urgent need for good quality urban climate monitoring networks (Muller et al., 2013).

The conditions prescribed for meteorological observations by WMO (2008) cannot be met in an urban environment due to the high density of buildings and other obstacles. This explains why the majority of meteorological measurement sites is located in rural areas. Specific measurement campaigns are therefore undertaken in cities spread over different climate zones to investigate the urban impact on the atmosphere (Oke, 2004). Depending on the scope of the network and the available budget, different strategies can be followed for organizing in-situ urban observations. One could invest in a limited number of high-accuracy weather stations or use a multitude of cheap but less accurate sensors as is the case for crowd-sourced weather data (Meier et al., 2017). For the MOCCA network the first strategy is chosen.

Setting up an urban measurement campaign is complex, time-consuming and expensive, and once installed the network needs maintenance. For this reason multi-year high-accuracy measurement campaigns are rare (Muller et al., 2013). Some examples of urban observation campaigns are the Helsinki testbed (Koskinen et al., 2011), the BUBBLE campaign in Basel (Rotach et al., 2005), TOMACS in Tokyo (Misumi et al., 2019), the BUCL network in Birmingham (Chapman et al., 2015) and the URBAN-PATH networks in Szeged (Skarbit et al., 2017) and Novi Sad (Šećerov et al., 2015). Despite being one of the most urbanized countries in the world, Belgium did not have any urban climate monitoring network. Belgium does not have very large cities but is characterized by a widespread urbanization, especially in its northern region Flanders where in 2015 16% of the surface was paved. Given the importance of urbanization and the associated increase in built-up areas for this region, it was decided in 2016 to initiate urban climate monitoring network in the city of Ghent.

This manuscript has two objectives:

1) Presenting the MOCCA network which provides a long-term, accurate urban climate dataset. Detailed information on the site characteristics, sensors… is included.
2) Discussing the complementarity between an observational network and urban models. Two different modelling approaches to obtain urban climate information are used: 1 km resolution runs of the SURFEX land surface model and 100 m resolution runs of the computationally cheaper UrbClim boundary layer model. On the one hand, urban model climatologies are proposed as a tool to assist choosing locations for a monitoring network. On the other hand, screen level MOCCA observations are used to evaluate the modelled UHI for summer 2016.

The following section (materials and methods) starts with a short description of the study area. Subsequently, the MOCCA monitoring network is introduced including a detailed discussion of the site characteristics. The section ends with a description of the two urban climate modelling strategies that are used for this study. Section 3 presents the observed and modelled UHI intensity for summer 2016. The observed intra-urban UHI differences and the model performances are discussed in Section 4. This section also puts forward the potential of applying urban climate model output as a supporting tool for the selection of locations for an observational network. The paper ends with a conclusion highlighting the key findings and suggestions for future research.

2. Materials and methods

2.1. Study area

With a population of about 260,000 inhabitants within the city borders and about 560,000 inhabitants in the agglomeration (statbel.fgov.be, consulted on March 5, 2019), Ghent is a typical mid-size European city located in the North of Belgium at the confluence of the rivers Lys and Scheldt. The flat topography and Ghent not being a coastal city simplify the interpretation of meteorological observations. The region experiences a mild maritime climate with an average minimum and maximum temperature of 0.4 °C and 7.0 °C in January, and 13.2 °C and 23.0 °C in July (RMI, 2019). The average annual precipitation amounts to 859 mm.

Fig. 1 presents the study area. Ghent has a historical city centre characterized mainly by low-rise buildings. More to the outskirts of the city, the densely built and populated landscapes extend into suburban neighbourhoods with more detached houses interspersed by green patches. Suburban and rural landscapes are found outside of the city with an important exception being the port of Ghent in the north of the city.

2.2. Sensors and data collection

The meteorological sensors (from Campbell Scientific, United Kingdom), shown in Fig. 2, are mounted on a construction of 2 m height. Temperature readings are provided by a Pt-100 sensor placed in an actively ventilated radiation shield ((3) in Fig. 2). The stations are also equipped with a passively ventilated radiation shield ((1) in Fig. 2) containing a sensor measuring both relative humidity and temperature. An ultrasonic anemometer is used to determine the wind speed and wind direction ((4) in Fig. 2). Finally,

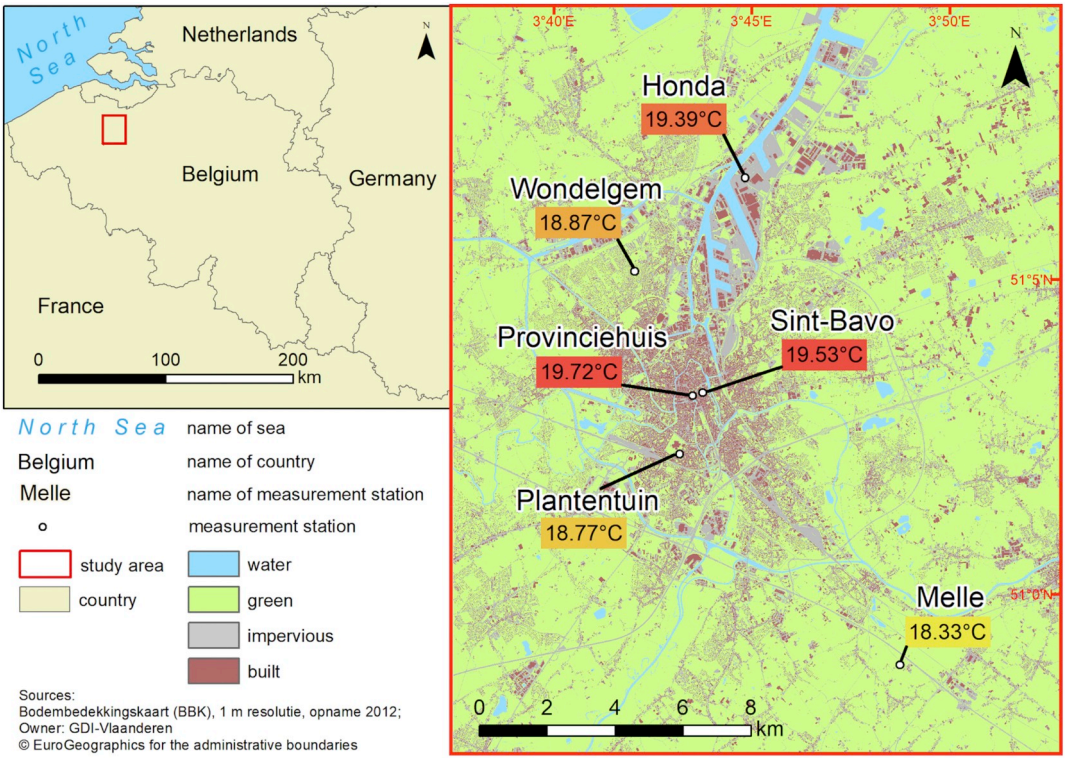

Fig. 1. Locations of the six MOCCA weather stations in the Ghent region. The average 2 m temperature measured during the July–August-September 2016 period is depicted for each MOCCA location.

Fig. 2. Sensors of a MOCCA weather station: (1) passively ventilated radiation shield containing a temperature and relative humidity sensor, (2) rain gauge, (3) actively ventilated radiation shield containing a temperature sensor and (4) ultrasonic anemometer.

a rain gauge ((2) in Fig. 2) is measuring precipitation. The guidelines drawn up by Oke (2004) have been used as a basis but for practical reasons it was not possible to follow them strictly at all times. Firstly, wind measurements at 10 m height are for practical reasons difficult in the city and it was therefore decided to mount the anemometer at 2 m height. As the wind field in the UCL is strongly disturbed by buildings and other obstacles, the readings of wind speed and direction differ from the measurements of nearby synoptic stations. Nevertheless, these measurements are useful for case studies because for some applications (e.g. thermal comfort studies, climate impact on buildings, …) one might be specifically interested in such screen-level wind measurements that are strongly affected by the micro-environment. Secondly, the exact locations have been chosen on the basis of their representativeness for the temperature measurements and these are not necessarily the best locations for precipitation measurements. It was practically impossible to perform the precipitation measurements at a different location as proposed by (Oke, 2004). However, the adverse effect on the MOCCA precipitation measurements seems to be very limited except in the botanical garden during the leafy season. Further

Table 1
Technical specifications of the sensors of the MOCCA stations. The accuracies are provided by the manufacturer.

	Sensor type	Accuracy	Remarks
Temperature	PT100 PRT probe	0.1 °C @ 0 °C	in actively ventilated radiation shield
Temperature	HC2S3 probe	0.1 °C @ 23 °C	in passively ventilated radiation shield
Relative humidity	HC2S3 probe	0.8%	in passively ventilated radiation shield
Wind speed	WindSonic 1	2% @ 12 m/s	at 2 m height
Wind direction	WindSonic 1	3 °	at 2 m height
Precipitation	ARG100 tipping bucket rain gauge	depends on precipitation type and intensity	0.2 mm resolution

specifications about the sensors can be found in Table 1. A data logger (type CR6 Campbell Scientific) is used to collect the sensor readings. The weather station needs electricity for the data logger, sensors and communication module. In case of an electricity cut a battery temporarily takes over the energy supply.

To ensure that all sensors are working properly and according to the specifications given by the manufacturer, the automatic weather stations were first located next to a WMO compliant synoptic weather station. This confirmed the specifications except for the passively ventilated temperature measurements which showed unexpected large biases. Therefore, the UHI intensity analysis presented in the next section, will be solely based on the actively ventilated temperature readings.

Measurements are taken at a temporal frequency of 1 measurement per second, but only 1 min.

averages are stored. Data are communicated to the server via GPRS. Each day the 1-min observations are transferred at midnight and, additionally, 5-min averages are sent every 5 min to permit a near real-time monitoring. The near real-time data availability is chosen for two reasons:

- It permits a close monitoring of the measurements and any incident (broken sensor, electricity cut, …) can be quickly detected avoiding significant data gaps.
- It enables near real-time visualization of the observations on the website (www.mocca.ugent.be) increasing the visibility of and involvement in the project for local residents, host institutions, stakeholders, …

The clock time of each data logger is recalibrated daily by communication with a NTP server, in.
this way the time consistency between the different stations is guaranteed.

2.3. Monitoring network and site characteristics

The monitoring network consists of 6 automatic weather stations spread over the study area. The MOCCA stations are located such that they sample diverse landscapes as illustrated in Fig. 3. In order to improve the usefulness of observational climate studies, different authors introduced classifications that go beyond the urban - rural division of measurement sites (Ellefsen, 1990-1991; Theurer, 1999; Oke, 2004). The classification based on the local climate zone (LCZ) scheme (Stewart and Oke, 2012) is used most often in climate studies. The LCZ classification scheme is developed to improve inter-site comparisons for UHI research, and to provide an objective protocol for reporting on UHI intensity. The scheme consists of 17 standard LCZs, divided into built (1 to 10) and natural zones (A to G), with a unique air temperature regime below mean roof level under similar atmospheric conditions (Stewart et al., 2014). The different zones are characterized by a unique set of properties linked to building height, building density, the zone's function and land cover. The LCZ map for Ghent, shown in Fig. 3, allows for a discussion of the different landscapes in the study area and the monitoring sites (Verdonck et al., 2017).

The study area consists of 9 different LCZs; 5 built and 4 natural zones can be distinguished. The locations *Provinciehuis* and *Sint-Bavo,* located in the core of the city, are mainly covered by compact mid-rise and compact low-rise zones (LCZ 2 and LCZ 3), which are densely built and populated. Some parks can be recognized in the city centre; station *Plantentuin* is located in one of them. The outskirts of the city, dominated by suburban neighbourhoods consist of open low-rise and sparsely built zones (LCZ 6 and LCZ 9). The suburban *Wondelgem* location is mainly characterized by an open low-rise built environment (LCZ 6). The port region, north of the city centre, is a large industrial zone mapped as large low-rise (LCZ 8) and is represented in the network by location *Honda*. However, small areas of large low-rise are scattered through the whole built-up zone in Ghent. Outside of the built-up area, the rural areas are dominated by low plants (LCZ D) explaining the choice for the *Melle* location as a rural reference. Forested areas are scarce in the surroundings of Ghent as illustrated by the low fractions of dense trees and scattered trees (LCZ A and LCZ B). Zones such as e.g. compact high-rise, bare rock or open high-rise do not occur or are not large enough in the study area to establish a local climate.

Table 2 provides an overview of the location characteristics of the different monitoring sites. The land cover is derived from the *Bodembedekkingskaart* (BBK) that covers Flanders at 1 m resolution (Agentschap Informatie Vlaanderen, 2016). The sky view factor (SVF) is calculated by using RayMan (Matuschek and Matzarakis, 2010; Matzarakis et al., 2010). Pictures of each measurement station, detailed maps with the land cover for different buffer radii, land cover fractions and a description of each station are included in the Appendix.

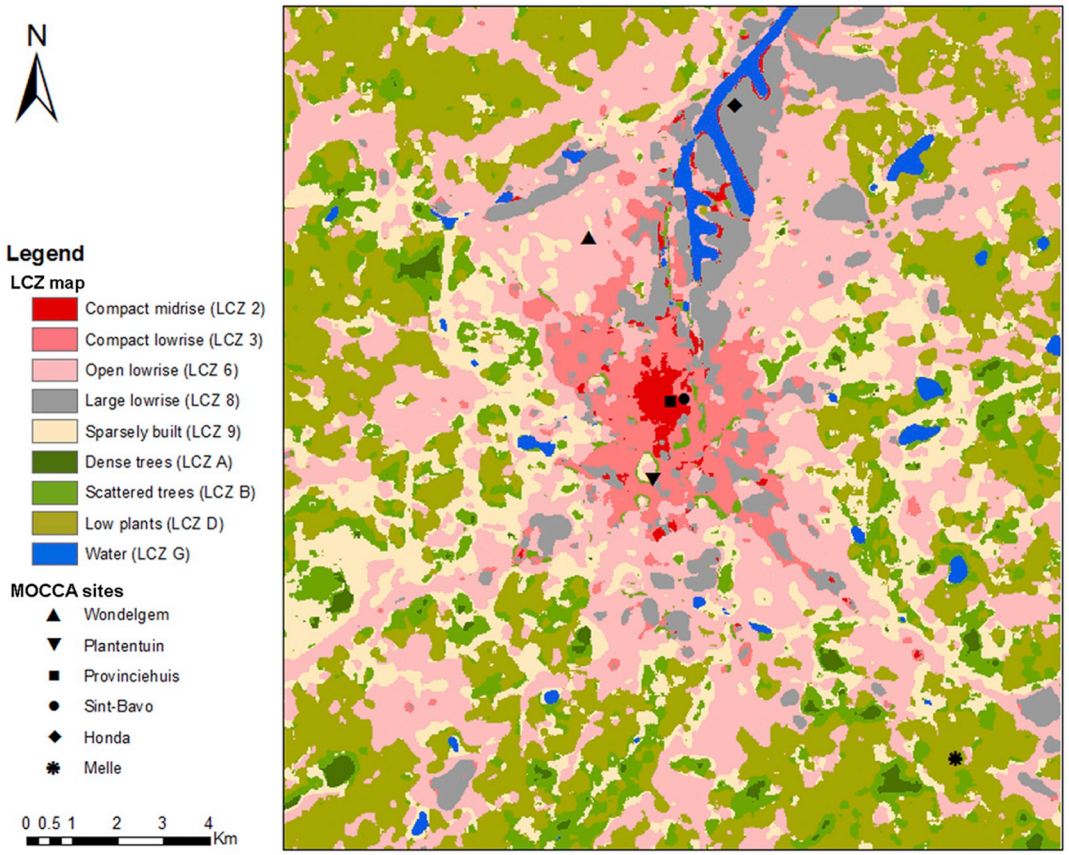

Fig. 3. Overview of the MOCCA network on a local climate zone map of the study area.

Table 2
Site characteristics for the locations of the MOCCA network.

Name station	Lon. WGS84 (^{0})	Lat. WGS84 (^{0})	Alti- tude (in ASL)	Land cover fraction (at 1 km^2 scale)				Aver. building height at 1 km^2 scale (in m)	SVF at station location (%)	LCZ
				% green	%impervious		% water			
						%buildings				
Honda	3.749	51.109	8	4	76	18	20	17	63.9	8
Wondelgem	3.703	51.084	8	60	40	17	0	7	46.5	6
Sint-Bavo	3.732	51.052	7	13	80	45	7	18	18.5	3
Provinciehuis	3.728	51.051	9	7	88	51	5	20	59.5	2
Plantentuin	3.722	51.036	18	35	65	34	0	15	39.3	9
Melle	3.816	50.980	15	91	9	2	0	7	100	D

2.4. Urban modelling

Two different urban modelling strategies are applied in this study. Fig. 4 visualizes how both approaches downscale ERA-Interim reanalysis data (Dee et al., 2011) to the urban scale. The procedures can be found in the following subsections and the references therein. As an illustration both methodologies are applied to create an UHI climatology over the Ghent region. These two downscaling setups will be used in Section 3.2 to model the UHI intensities over the study area for July-August-September (JAS) 2016.

2.4.1. The ALARO-SURFEX setup

This downscaling procedure is based on simulations of the land surface scheme SURFEXv5 coupled to the regional climate model ALARO-0, a configuration developed within the ALADIN system (Termonia et al., 2018). The experimental setup is briefly described, for more details the reader is referred to Hamdi et al. (2014) and Hamdi et al. (2015).

The ALARO-0 regional climate model uses a physics parameterization specifically designed to be run at convection-permitting resolutions. Its key concept lies in the so-called Modular Multiscale Microphysics and Transport (3MT) scheme handling the

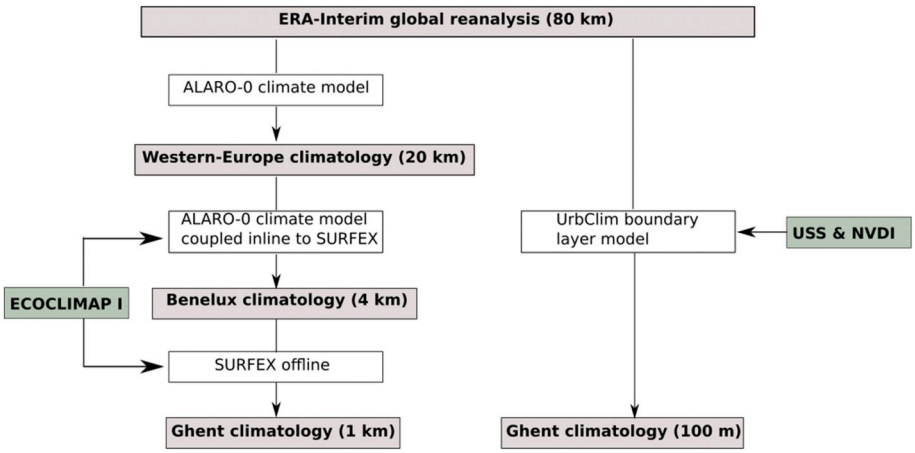

Fig. 4. The ALARO-SURFEX (left) and UrbClim (right) setups to downscale ERA-Interim reanalysis data to the urban scale over Ghent.

convection, turbulence and microphysics (Gerard and Geleyn, 2005; Gerard, 2007; Gerard et al., 2009). In the externalized land and ocean surface platform SURFEX (SURface Externalisée; (Masson et al., 2013)) each grid box consists of four tiles associated with a specific parameterization: nature, urban areas, sea or ocean, and lake. The Town Energy Balance single-layer urban canopy model, or shortly TEB, is used for urban tiles (Masson, 2000). Horizontal interaction does not exist between the different surface area tiles. The land cover types include 14 classes provided by the ECOCLIMAP I database (Masson et al., 2003). The SURFEX model can be used in two modes. One could run SURFEX in a so-called inline mode for which surface fluxes and atmospheric forcings are exchanged at every time step with a numerical weather prediction (NWP) or climate model. Or it can be used in an offline mode where the atmospheric drivers are derived from NWP or climate model output and fed to the surface scheme without any feedback to the atmospheric model. For the setup used here, SURFEX is used in both modes as shown in Fig. 4.

The procedure used for the ALARO-SURFEX downscaling uses three domains. Both the 20 km and 4 km domains are vertically divided into 46 layers with the height of the lowest layer centred at about 17 m above the ground. Firstly, the ERA-Interim data are used to drive the ALARO-0 climate model on the 20 km domain whose output is on its turn used to drive a 4 km ALARO-0 run in an inline mode coupled to SURFEX. In order to further downscale to an urban scale the SURFEX land surface modelling system is employed on the 1 km resolution domain in offline mode using the forcing coming from the lowest model level of the 4 km simulations. As in the experimental setup described by Hamdi et al. (2015) and Hamdi et al. (2016), SURFEX offline is coupled to a surface boundary layer (SBL) scheme following the methodology described in Hamdi and Masson (2008) and Masson and Seity (2009). Six

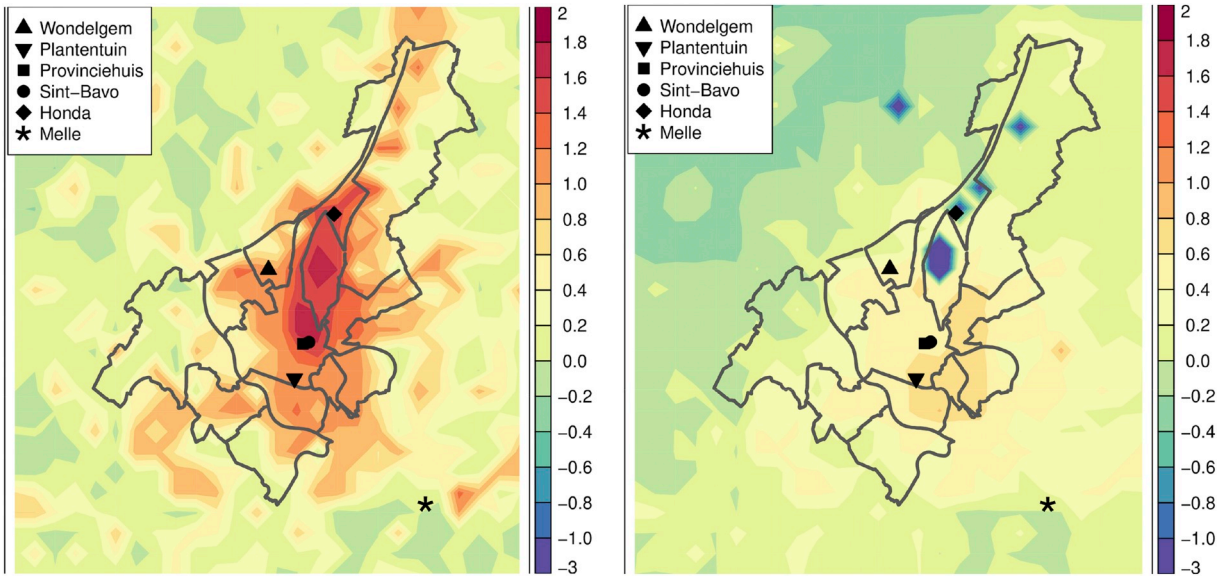

Fig. 5. Average JAS nighttime (left) and daytime (right) UHI derived from multi-year ALARO-SURFEX downscaling of ERA-Interim reanalysis. The UHI intensity is defined with respect to the average temperature of all grid points qualified as rural. The locations of the MOCCA stations are shown.

prognostic air layers (0.5, 2, 4, 6.5, 10, and 17 m above the ground) are therefore added from the ground up to the lowest ALARO level which is the forcing level.

Fig. 5 presents the UHI climatology for JAS derived from the ALARO-SURFEX setup for the period 1991–2010. The modelled climatology confirms the dual role of water found by previous observational (e.g. Steeneveld et al., 2014) and modelling studies (e.g. Theeuwes et al., 2013); water surfaces provide cooling during the day but during summertime nights the temperature remains relatively high.

2.4.2. The UrbClim setup

The urban boundary layer climate model UrbClim (De Ridder et al., 2015) is designed to cover agglomeration-scale domains at a high spatial resolution, taken as 100 m for this study. UrbClim consists of a land surface scheme containing simplified urban physics, coupled to a 3-D atmospheric boundary layer module. The latter is tied to synoptic-scale meteorological fields through the lateral and top boundary conditions, to ensure that the synoptic forcing is properly taken into account. The land surface scheme is based on the soil-vegetation-atmosphere transfer scheme of De Ridder and Schayes (1997), but is extended to account for urban surface physics. This urbanization represents the urban surface as a rough impermeable slab, with appropriate values for the albedo, emissivity, thermal conductivity and volumetric heat capacity. The main feature of the extension of the scheme is the inclusion of a parameterization of the inverse Stanton number, which is known to be much higher in urban areas (Kanda et al., 2007; De Ridder et al., 2012). A full description of the UrbClim model can be found in De Ridder et al. (2015).

The spatial distribution of land cover types, needed for the specification of required land surface parameters, is taken from the reference land use map for Flanders, described in White et al. (2015). The percentage of urban land cover is specified using the Urban Soil Sealing (USS) raster data files distributed by the European Environment Agency. Maps of vegetation cover fraction are obtained from the Normalized Difference Vegetation Index (NDVI) acquired by the MODIS instrument on-board the TERRA satellite platform. Vegetation cover fraction is specified as a function of the NDVI using a linear relationship proposed by Gutman and Ignatov (1998), and then interpolated to the model grid. Model grid cells featuring exclusively non-urban land use types are divided into vegetation and bare soil (the complementary fraction). In the case of grid cells containing urban land use, the urban fraction as derived from the Soil Sealing data takes precedence over the NDVI-based fractional vegetation cover data in case both sum to over 100%. In case they sum to less than that, the remaining fraction is assigned to bare soil. Terrain elevation data are taken from the GMTED2010 Dataset (Danielson and Gesch, 2011), which has a global coverage and is freely available.

Fig. 6 is based on simulations of the UrbClim setup for JAS 2000–2015 over a domain encompassing the study area. The model is driven directly with meteorological data from the ERA-Interim reanalysis, as was the setup in previous validation experiments (De Ridder et al., 2015; García-Ddíez et al., 2016; Lauwaet et al., 2016; Lauwaet et al., 2017). The model domain is configured with 301 by 301 grid cells in the horizontal direction, using a spatial resolution of 100 m. In the vertical direction, 20 levels are specified, with the first level 10 m above the displacement height, the resolution smoothly decreasing upward to 250 m at the model top located at 3 km height. This vertical discretization closely matches that of the ECMWF host model. The 2 m temperature, which is needed for canopy UHI studies, is diagnostically estimated by an extrapolation from the lowest model level using profile functions (De Ridder et al., 2015). The simulation is initialized each year on 1 May at 0000 LT, resulting in a two-month spin-up before the start of the analysis on 1 July, in order to ensure model equilibrium between external forcings and internal dynamics, especially in terms of soil variables. Initial soil temperature and soil moisture data are taken from the ERA-Interim reanalysis.

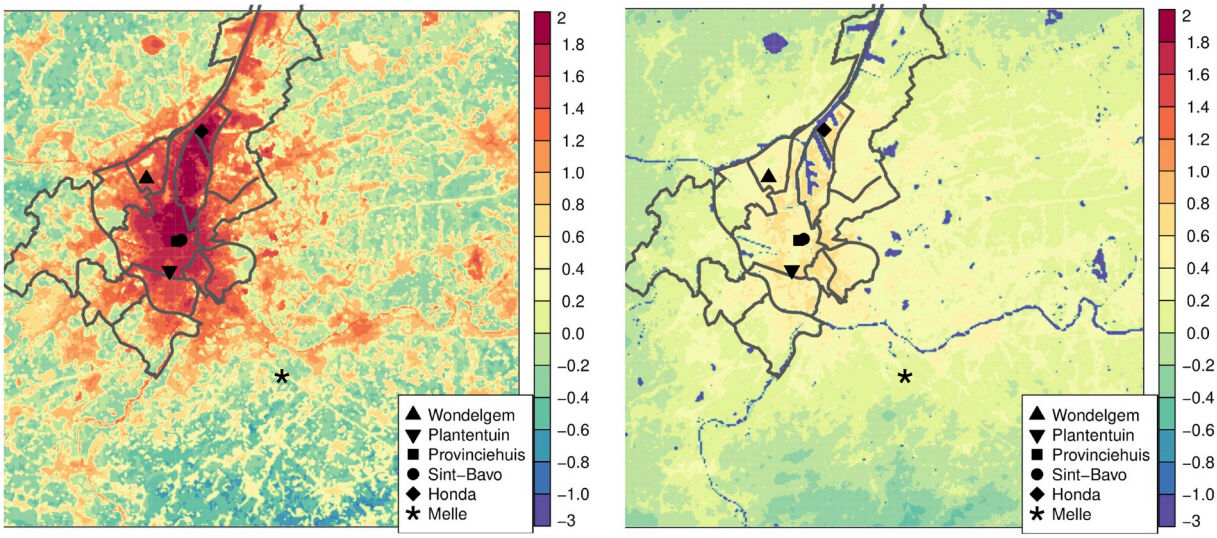

Fig. 6. Average JAS nighttime (left) and daytime (right) UHI derived from multi-year UrbClim downscaling of ERA-Interim reanalysis. The UHI intensity is defined with respect to the average temperature of all grid points qualified as rural. The locations of the MOCCA stations are shown.

3. Results

In this section the observed and modelled UHI intensity, defined here as the temperature difference with the rural location *Melle,* is analysed at the MOCCA locations for JAS 2016.

3.1. Observed UHI intensity for JAS 2016

Fig. 7 shows the 2 m actively ventilated temperature measured in *Melle* and the temperature difference between *Sint-Bavo*, located in the narrow urban canyon which is representative for the city center, and *Melle* during the study period. During nights characterized by clear and calm meteorological conditions UHI intensities up to 6 °C are observed. The daytime temperature at *Sint-Bavo* is on average slightly higher than at *Melle*. The few negative temperature differences in Fig. 7 are linked to fronts coming from the west that reach *Sint-Bavo* before *Melle*.

The average daily cycle of the observed canopy temperature and UHI intensity for the different measurement locations is shown in Fig. 8. The largest UHI intensity occurs shortly after sunset and is followed by a slow decrease until the morning. After sunrise the temperature in *Melle* is catching up quickly with the temperature at the more urbanized locations. The observed intra-urban temperature differences confirm that a city consists of different LCZs. *Provinciehuis* and *Sint-Bavo*, located both in the city centre, show similar nocturnal temperature curves with a maximal average UHI intensity of +2.5 °C. The harbor location *Honda* has a slightly lower average peak intensity (+2.2 °C). *Plantentuin* and *Wondelgem* have more limited nighttime UHI intensities e.g. the peak UHI intensity of *Wondelgem* (+1.2 °C) is about half the one measured in the city centre.

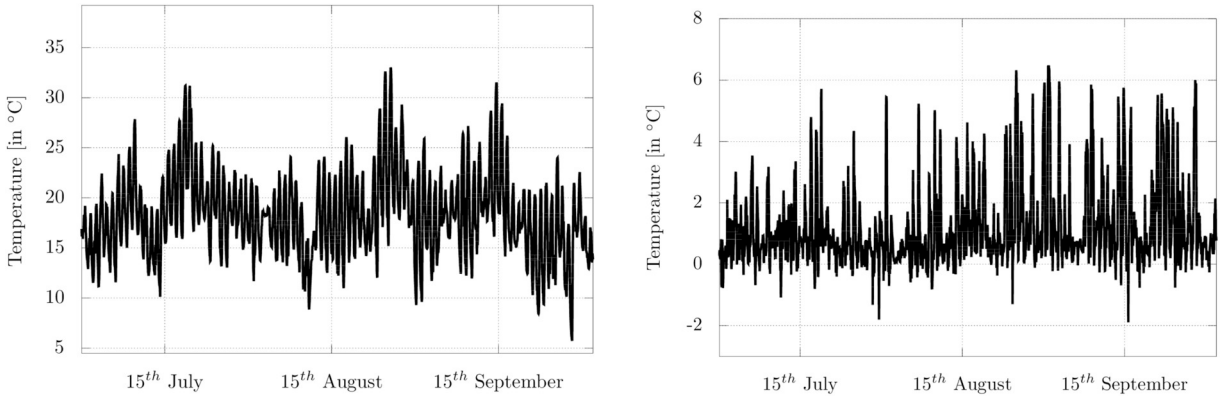

Fig. 7. MOCCA time series of 2 m temperature in *Melle* (left) and temperature difference between *Sint-Bavo* and *Melle* (right) for JAS 2016. Hourly averaged values are used.

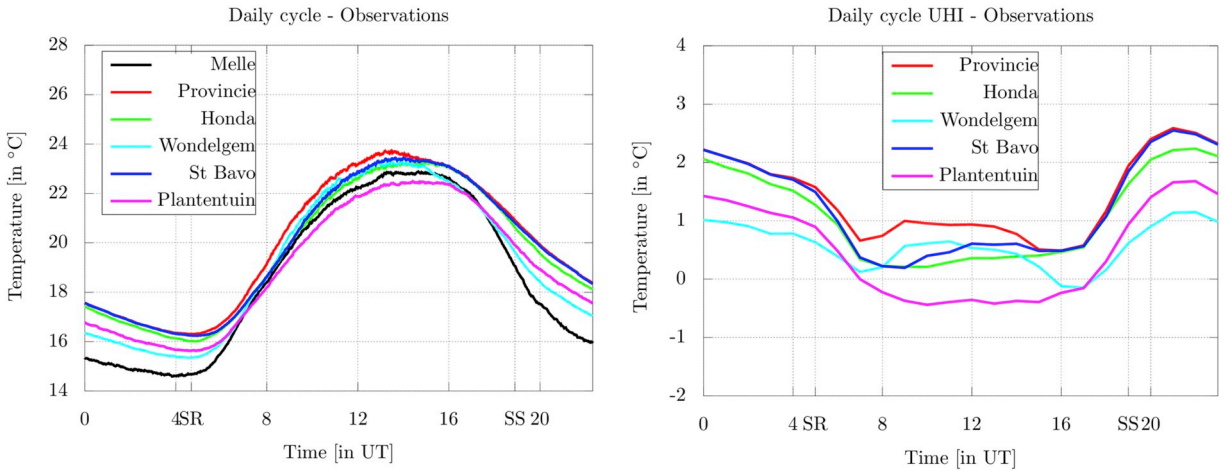

Fig. 8. Daily cycle of actively ventilated 2 m temperature (left) and UHI intensity defined as the temperature difference with the 2 m temperature in *Melle* (right). The time of sunrise (SR) and sunset (SS) is shown on the horizontal axis.

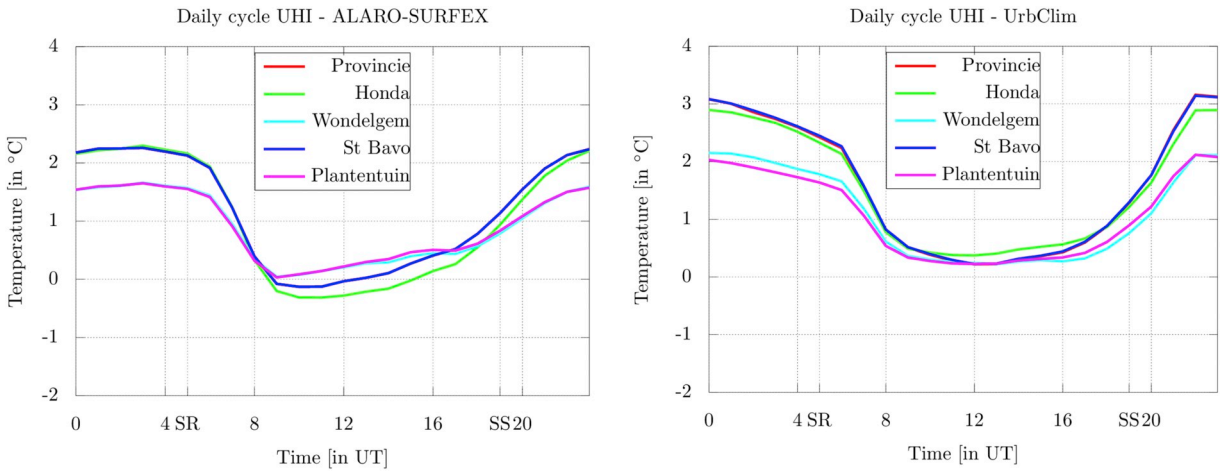

Fig. 9. Average daily cycle of modelled UHI intensity with respect to 2 m temperature in *Melle* for ALARO-SURFEX (left) and UrbClim (right). The time of sunrise (SR) and sunset (SS) is shown on the horizontal axis.

During the day the urban weather stations register only limited temperature differences with respect to *Melle*. The peak daytime UHI intensities averaged over the evaluation period vary between −0.5 °C (*Plantentuin*) and + 1 °C (*Provinciehuis*). Despite the limited magnitude of the daytime temperature differences, interesting patterns are recognized. For example, at the locations of *Provinciehuis* and *Wondelgem* the UHI intensity is increasing in the morning towards a relative maximum before noon. Such a before noon maximum is not found at other urban locations.

3.2. Modelled UHI intensity for summer 2016

Fig. 9 shows the average daily cycle of the modelled UHI intensity for the urban locations obtained by applying the UrbClim and ALARO-SURFEX downscaling procedure as described in Section 2.4. Note that the location of *Provinciehuis* and *Sint-Bavo* share the same closest gridpoint in the 1 km resolution ALARO-SURFEX runs. Both model setups show significant intra-urban UHI intensity differences during the night. Two clusters can be distinguished:

1) The locations *Provinciehuis, Sint-Bavo* and *Honda* have average nighttime peak UHI intensities just over 2 °C for ALARO-SURFEX and 3 °C for UrbClim. The corresponding observed value is 2.5 °C for *Provinciehuis* and *Sint-Bavo* and 2.2 °C for *Honda*.
2) The locations *Wondelgem* and *Plantentuin* have similar modelled UHI intensities around 1.5 °C for ALARO-SURFEX and 2 °C for UrbClim. The observations reveal a higher UHI intensity in the *Plantentuin* (1.5 °C) than at *Wondelgem* (1.2 °C).

In both model setups the temperature differences build up fast around sunset and disappear shortly after sunrise. The UrbClim setup results in a peak intensity in the evening followed by a steady decrease which agrees with the observed evolution. The ALARO-SURFEX setup expects a constant UHI intensity during the night. During the day both model experiments result in limited, mostly positive UHI intensities with little intra-urban spread. In the ALARO-SURFEX setup a minimal UHI intensity, even negative at some locations, is reached before noon. None of the models is able to reproduce the observed intra-urban daytime temperature differences.

The averaged UHI intensities from a multi-month period, as shown in Fig. 9, may hide underlying weaknesses like large daily outliers. Therefore the root mean square errors (RMSE) of the model output with respect to the observations are included in the Appendix. The values are separately calculated for the day and night to avoid compensating errors. The RMSE values are similar for both models and slightly lower during the day (about 1 °C) than during the night (about 1.5 °C).

4. Discussion

4.1. Evaluation of observed and modelled intra-urban UHI intensity

Earlier studies, e.g. Brandsma and Wolters (2012), concluded that nighttime UHI intensities can be explained by local scale characteristics. For each measurement location the land cover fractions for a 565 m radius source area, corresponding with a 1 km^2 area and representing the local scale, are summarized in Table 2. The observed nighttime UHI pattern correlates well with the

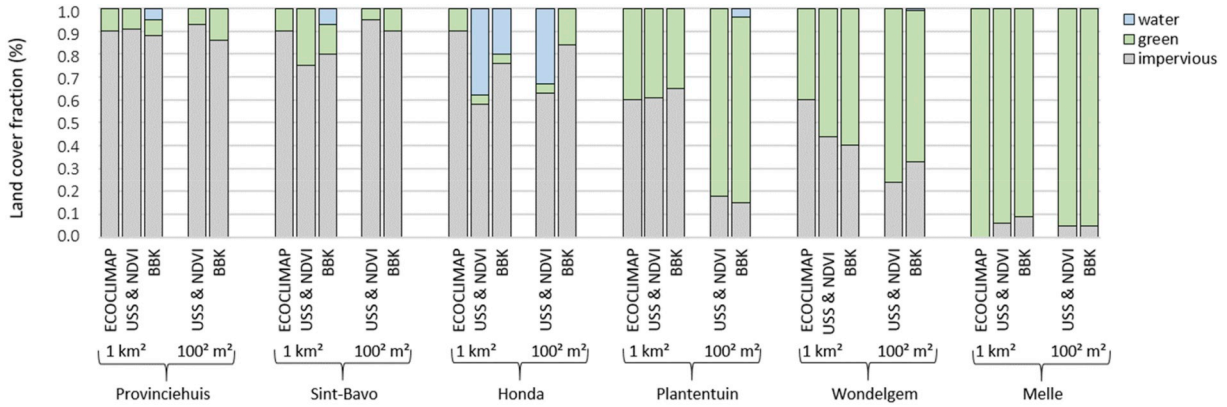

Fig. 10. Land cover around the measurement stations based on ECOCLIMAP I (used by ALARO-SURFEX), USS & NDVI (used by UrbClim) and BBK database both for the 100 m × 100 m and 1000 m × 1000 m grid cells.

impervious fraction on the local scale: the larger the impervious fraction, the stronger the observed UHI intensity. Despite being an urban park the location *Plantentuin* is more impervious at the local scale than the suburban *Wondelgem* which explains the on average larger nighttime UHI at *Plantentuin*. Similarly an inverse correlation exists between the nocturnal UHI intensity and the green fraction. Conclusions on the impact of water surfaces cannot be made as only the *Honda* location has a considerable fraction of water. Van Hove et al. (2015) concluded for the city of Rotterdam that the built fraction is the strongest predictor of the nocturnal UHI. This is in contradiction with the MOCCA measurements at the port location of *Honda*. This industrial environment combines large concrete surfaces with few buildings (18% of the 1 km^2 area) and is characterized by a 76% fraction of impervious surfaces (only slightly lower than the city centre). Despite the open landscape and the corresponding efficient nocturnal radiative cooling, UHI intensities close to the ones in the city centre are found. Because of this location no significant correlation between built surface and UHI intensities is found for the Ghent region. This apparent contradiction with Van Hove et al. (2015) might be explained by the fact that this type of environments (impervious with few buildings) is not so common and often not included in urban measurement networks.

During the day most urban locations have a limited positive UHI intensity except for the urban park location. It is found that daytime UHI patterns can be understood by analysing the location's micro-environment. Detailed maps and land cover fractions for the microscale are included in the Appendix. The limited negative UHI intensity during most of the day at location *Plantentuin*, which was also measured during an earlier measurement campaign in Ghent (Maiheu et al., 2013), is probably linked to the dense, irrigated vegetation that provides shading and increased evapotranspiration reducing the sensible heat (Wang et al., 2015). A more in-depth study of the microclimate at location *Plantentuin* would be valuable as urban green is considered as one of the main UHI mitigation strategies. The microscale environment also explains the before noon UHI intensity maximum at *Provinciehuis* and *Wondelgem.* Both weather stations are located nearby a building with eastern oriented walls. The quick response of these walls to the morning solar radiation explains the relative UHI intensity maximum before noon.

The previous analysis shows the importance of using appropriate landscape information for urban climate model experiments. Apart from the different methodologies and resolutions, both model setups use different land databases as illustrated in Fig. 4. A comparison of the land cover fractions used by both models is presented in Fig. 10. The models are performing reasonably well for the nocturnal UHI intensity:

- The UrbClim model is slightly overestimating the nocturnal UHI for all locations. This might also be related to the modelled temperature at the rural location. The climatology maps illustrate that both setups result in very similar spatial patterns for the nocturnal UHI maps. At the suburban *Wondelgem* location both models overestimate the UHI intensity. This is probably linked to an overestimation of the impervious fraction in the land use databases used by both model setups e.g. 60% ECOCLIMAP-I versus 40% BBK for the *Wondelgem* location.
- The observations show a peak UHI intensity shortly after sunset (around 21 UT) followed by a steady decrease until the late morning. In the models the maximal UHI intensity is lagging the observations. Moreover, the decrease of the UHI intensity is too slowly resulting in an overestimation of the modelled UHI intensity around sunrise.
- Both models correctly estimate the large nocturnal UHI magnitude observed at *Honda*. Figs. 5 and 6 show that the models simulate a significant positive nocturnal UHI for the whole port region (also in the grid points where no water fraction is present) and therefore one can conclude that ALARO-SURFEX and UrbClim are able to estimate well the UHI in sparsely built, impervious landscapes.

During the day, except for the early morning and late evening, the models expect limited UCL temperature differences. At noon, for example, UrbClim and ALARO-SURFEX output shows UHI intensities in the range [0.2, 0.4] °C and [−0.3, 0.3] °C. As can be seen in Fig. 8 this is an underestimation of the [−0.3, 1.0] °C observed intra-urban temperature spread. This agrees with the fact that the microscale, which is not resolved by the models, dominates the daytime temperature evolution. Both models are based on parametrizations using average land cover, building properties… to model an average temperature over a grid box. Daytime temperature profiles linked to the presence of individual buildings are beyond the capabilities of these models.

Despite the fact that at 100 m resolution the land cover database used by UrbClim resolves the green area around the *Plantentuin* location, the model does not capture the observed negative daytime UHI. The UrbClim model may be underestimating the effect of shading by trees. Given the dimensions of the urban park, the 1 km resolution is too coarse to expect any impact for the ALARO-SURFEX methodology.

4.2. Urban modelling to select locations

Observations are often used to validate models, but one might also consider the reverse i.e. using model output to evaluate a monitoring network.

The choice of measurement locations is of key importance for urban climate observation networks. Installing a network is time-consuming and expensive and for reasons of consistency it is highly unwanted to move monitoring stations during the campaign. Therefore, the selection of the measurement sites should be well-thought and the chosen locations should be tailored towards the objectives behind the network. One motivation for urban networks is to provide an accurate database for the validation of modelled seasonal and spatial variability of the urban climate over the study area. As LCZs are defined according to canopy temperature behaviour, the LCZ map of the study area (Fig. 3) forms a sound basis to select appropriate locations for an UCL network (see e.g. Lelovics et al. (2014)). Also aerial images (e.g. Google Maps) are often used as a tool.

However, for two reasons one could go further and consult model based climatologies for the study area before deciding on the selection of measurement sites:

1. Urban models include surface cover and surface geometry information (information also included in LCZ classification or aerial images) to simulate the surface-atmosphere interaction but they also enable dynamical effects such as advection or urban circulations. As these are relevant for the urban climate (e.g. Bassett et al. (2016) for advection and Haeger-Eugensson and Holmer (1999) for thermal circulations), a model based climatology can add information not present in e.g. LCZ classifications.
2. Unexpected model results for a certain part of the study area could motivate to place a measurement station in this zone such that the model behaviour can be verified. In case model validation is important, this strategy enables to employ the limited resources in a more efficient way.

The first motivation only holds if the urban modelling strategy is able to represent these dynamical processes. The UrbClim approach for example does not permit such dynamical effects whereas the ALARO-SURFEX setup does only permit this at the 4 km resolution ALARO run.

The modelled UHI climatologies of the Ghent region (Figs. 5 and 6) have been consulted before deciding on the MOCCA locations. As an example, both maps show a clear extension of the region with large UHI intensity north of the city centre, where the port of Ghent is located. Despite its substantial distance from the city centre, the port is expected to reach nocturnal UHI intensities similar to the city centre. This is an interesting result as the port, classified as LCZ 8 or large low-rise, has quite different properties e.g. the sky view factor is much higher than in the LCZ 2 and LCZ 3 zones. A weather station in the port would thus enable to verify the large nocturnal UHI expected by the models.

Selecting location needs compromises between scientific motivations and practicalities. Based on the urban climatologies, it would have been desirable to place a station at the spot identified by the models to experience the maximal UHI intensity (north of *Provinciehuis* and *Sint-Bavo*). In this part of the city no host location for a long term observational installation was found, hence this idea had to be abandoned and two stations at the border of LCZ 2 and LCZ 3 were selected. One can thus assume that the observed maximal UHI intensity will be an underestimation of the maximum UHI for Ghent. For the rural location it was decided to choose a measurement site of the Royal Meteorological Institute (RMI) southeast of the city. Following Fig. 3 this location is classified as LCZ D but a highway and a few buildings are present (the LCZ 6 spot nearby the *Melle* location). It is clear from Figs. 5 and 6 that cooler spots can be identified around Ghent but the need for electricity made it impossible to measure at more remote, rural locations. This implies again that the temperature differences measured between the stations in the urban landscapes and *Melle* underestimate the maximal UHI intensity.

5. Conclusions

The MOCCA network, operational in the city of Ghent since July 2016, is presented. To enable a convenient use of these data by other researchers, the manuscript and the Appendix provides extensive metadata following the recommendations of Oke (2006), Stewart (2011) and Muller et al. (2013). In this manuscript we only used temperature observations of one season but the availability of other parameters (e.g. relative humidity, wind speed, …) and the multi-year duration of the network enable many more studies. As an illustration Vandemeulebroucke et al. (2019) used 1 year MOCCA data to demonstrate that the UHI phenomenon has a significant impact on the durability of historic constructions. A detailed discussion of the intra-urban differences of other parameters (e.g. relative humidity, …) in Ghent will be included in an upcoming study on intra-urban differences in thermal comfort.

An evaluation of the observed and modelled canopy UHI intensities for the city of Ghent is presented for JAS 2016. Two different methodologies were used to obtain high resolution urban climate information starting from ERA-Interim reanalysis data: the UrbClim approach (100 m resolution) and the ALARO-SURFEX approach (1 km resolution). The observed nocturnal UHI intensities are explained by the local scale land cover around the measurement location. Both urban modelling approaches resolve this scale and capture well the nocturnal UHI intensity and the intra-urban differences. This illustrates the importance of using accurate land cover, building geometry… characteristics when modelling the urban climate. During the day the urban park location has on average a negative UHI intensity in summer which is not reproduced by the models. The observed daytime intra-urban temperature differences do not agree with the model results. The differences in daytime temperature are partly explained by the microscale environment (e.g. individual buildings, trees…). The models used in this study are based on parameterization schemes to describe the interactions on grid box scale and can therefore impossibly reproduce such microscale variations.

The success of a network is strongly depending on a well-thought siting strategy corresponding to the purpose of the network. Traditionally the location choices are based upon aerial images or LCZ maps. This paper argues that modelled urban climate information of the study area might be an additional tool to determine suitable locations for weather stations. This is especially true if the observations will be used for urban model validation and the monitoring network consists of a limited number of stations.

The MOCCA monitoring network will remain operational during the following years and will be used as a reference network for future measurement campaigns. As an example, citizen weather stations can provide interesting urban climate information but a limited, high-accuracy background network is needed for the quality control (Meier et al., 2017). An interesting extension to the current stationary network would be a set of easy-to-move weather stations (e.g. working on solar energy and wireless data communication) and use them for specific short-term measurement campaigns. One application of such a flexible network could be to investigate the impact of the exact location on the measurements. As discussed the microscale landscape determines the daytime temperature observations. Non-stationary weather stations provide a powerful tool to investigate and quantify the impact of the microscale on a particular location. For the MOCCA network, such stations would enable short term measurement campaigns in the urban canyon at *Provinciehuis* location to get more detailed insight in the changes in canopy temperature within the canyon or at *Plantentuin* to verify the robustness of the negative daytime UHI. Such campaigns are also an interesting test of the recommendations for the siting of urban measurement stations (Oke, 2004). Moreover flexible campaigns, together with the background MOCCA data, can also be used to investigate phenomena that cannot be investigated with the current stationary network e.g. UHI advection or the intra-rural differences.

All MOCCA data are available upon request and the authors hope that colleagues or scientists from other disciplines will take the opportunity to use the dataset for their research.

Declaration of Competing Interest

None.

Acknowledgment

The authors would like to thank the sponsors of this project (Department Physics and Astronomy of Ghent University, Farys and Observatory Armand Pien) and the partners hosting a MOCCA station. Thanks to Peter Camps for the high-quality photos of the MOCCA stations. Many thanks to Dragan Milosevic (University of Novi Sad) for the RayMan modelling. M.L. Verdonck is funded by the UrbanEARS project of the Belgian Federal Science Policy Office. We are grateful for the remarks and suggestions of the anonymous reviewers.

Appendix A. Appendix

A.1. Photos measurement sites

Impression of the MOCCA measurement locations. From left to right, top to bottom: *Sint-Bavo, Provinciehuis, Plantentuin, Melle, Wondelgem* and *Honda*.

A.2. High-resolution land cover maps for measurement sites

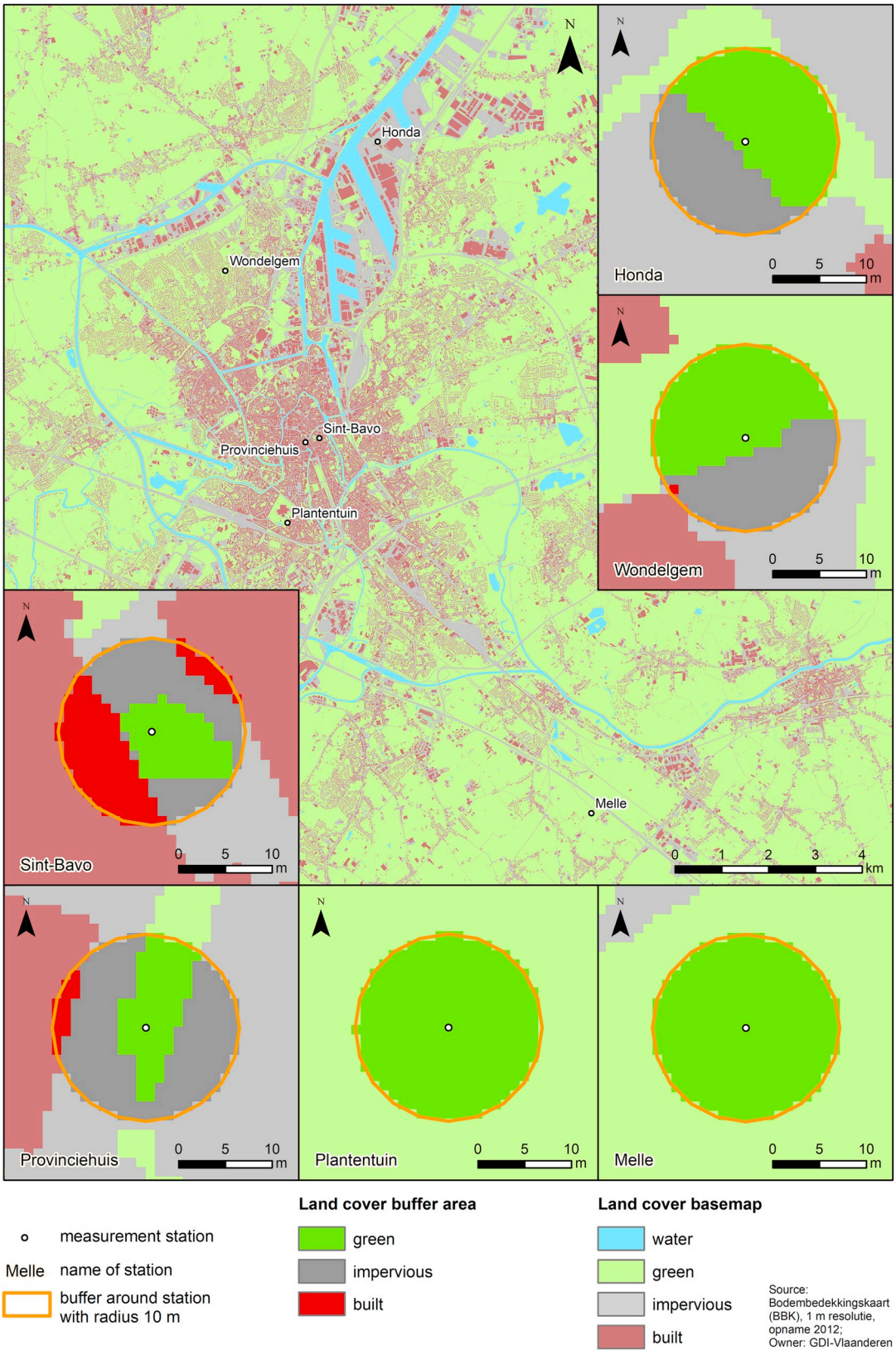

Land cover (1 m resolution) within 10 m radius around the measurement stations.

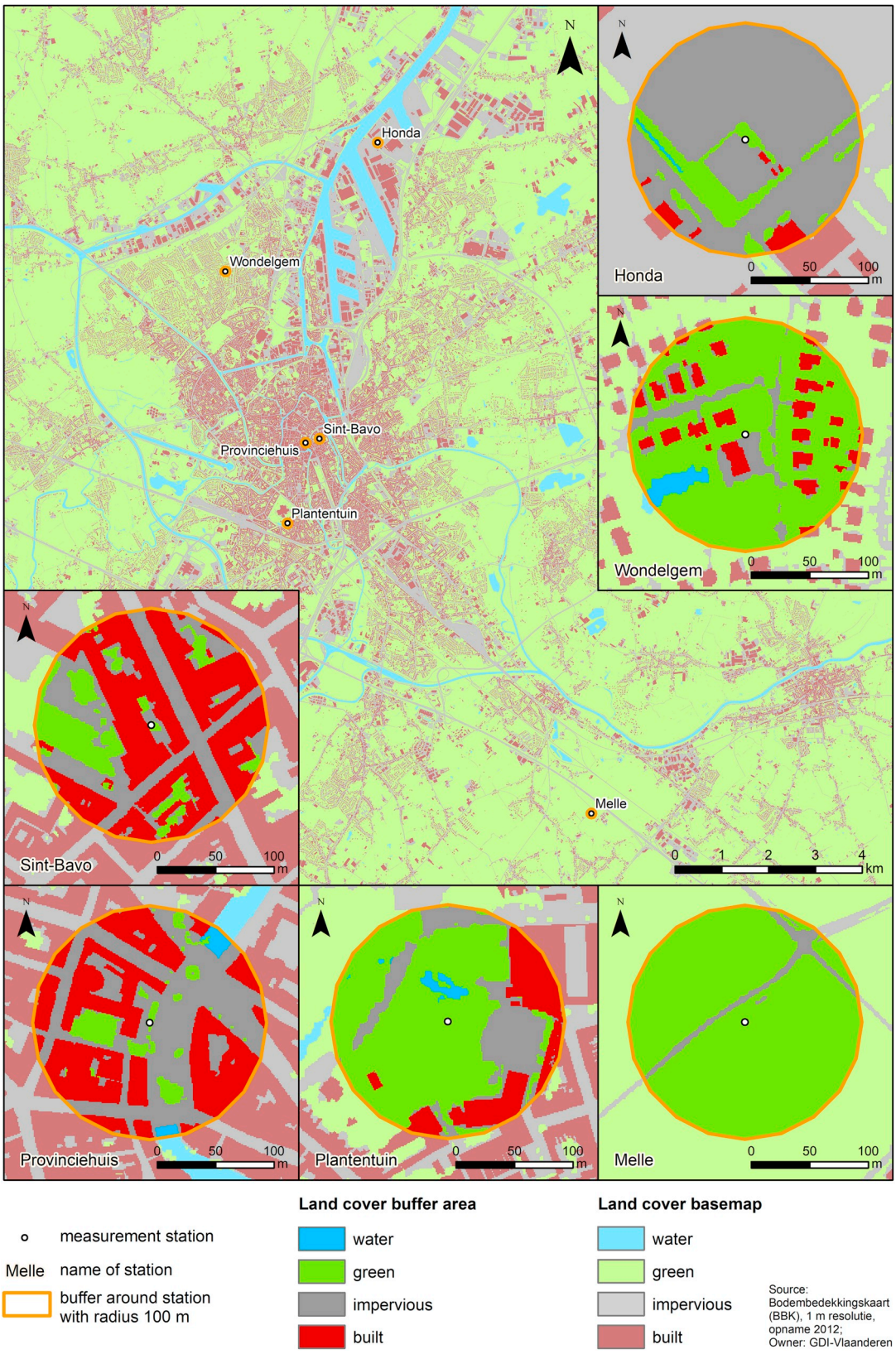

Land cover (1 m resolution) within 100 m radius around the measurement stations.

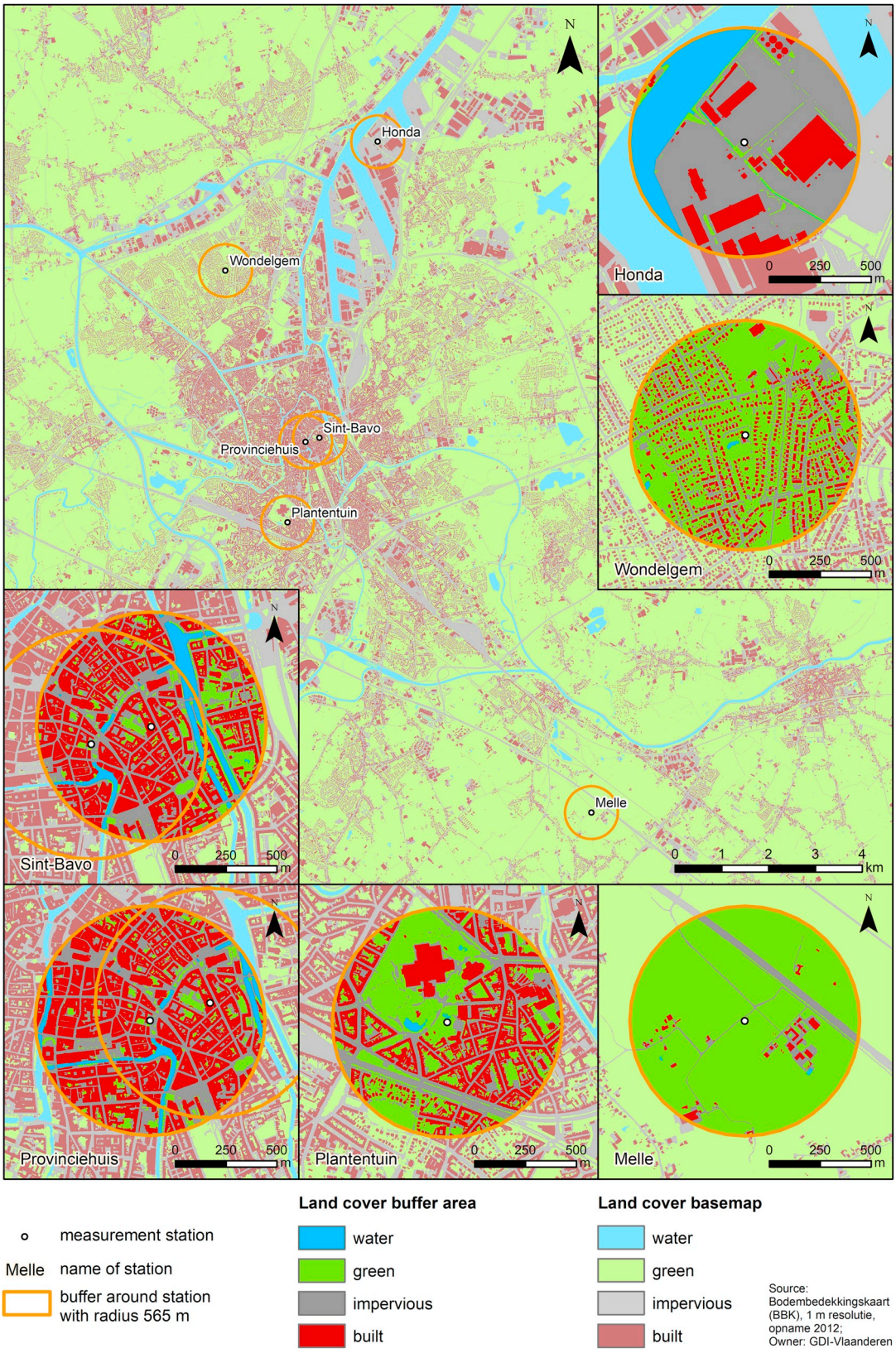

Land cover (1 m resolution) within 565 m radius around the measurement stations.

A.3. Land cover statistics for different radii around the MOCCA stations

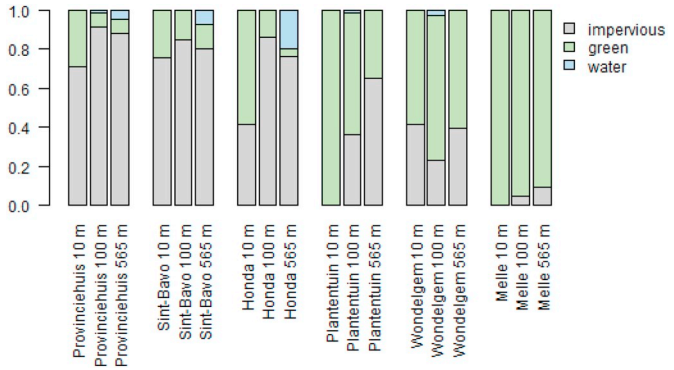

Aggregated land cover classes derived from the BBK dataset for the buffer radii of 10 m, 100 m and 565 m around the MOCCA stations.

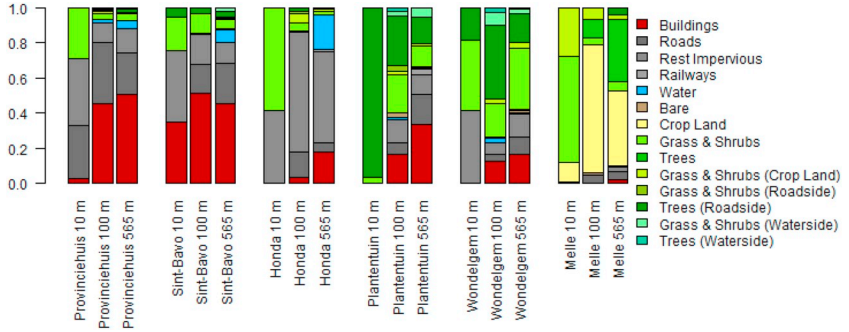

Detailed land cover fractions derived from the BBK dataset for the buffer radii of 10 m, 100 m and 565 m around the MOCCA stations.

A.4. Description of the MOCCA measurement locations

The **Honda** station (LCZ 8) is located at a small lawn surrounded by extensive asphalted terrains and industrial buildings. The location is very open, but a row of trees northeast of the weather station limits the sky view factor (SVF) to 0.64. The local scale environment is dominated by impervious land cover reaching a value of 86% at the 100 m buffer distance which is very similar to the locations in the city center. The lower impervious fraction for the microscale (41% for 10 m buffer radius) is explained by the small lawn, whereas at 565 m radius the impervious fraction is slightly decreased (76%) at the expense of water (the docks and canal of the harbor) and green (gardens in suburban landscapes).

The **Wondelgem** station (LCZ 6) is located above a lawn near a small square with parking lots, which is surrounded by greenery. This environment differs strongly from the Honda location since it is located in a suburban neighbourhood with open low-rise buildings (average building height 7 m). There are more buildings and trees in this area compared to the Honda location, explaining the smaller SVF (0.46) at the location of the Wondelgem measurement station. Both the microscale and local scale are dominated by pervious land cover (59% at 10 m radius, 74% at 100 m radius) due to the gardens around the houses and the green infrastructure along the roads.

The **Sint-Bavo** station (LCZ 3) and **Provinciehuis** station (LCZ 2) are located in the densely built city centre with only 300 m distance between them. Both locations have very similar properties on the local scale with on the 1 km^2 scale an impervious fraction of 80% versus 88%, Sint-Bavo being slightly greener. The average building height at this scale is 18 m (Sint-Bavo), respectively 20 m (Provinciehuis), which is similar to the Honda station but the fraction of buildings is very different: 18% at Honda versus 51% and 45% at Provinciehuis and Sint-Bavo. The micro-scale of both city center locations is very different. The Sint-Bavo station is located between two buildings, which form a narrow urban canyon resulting in the lowest SVF (0.18) of all locations. The Provinciehuis weather station is situated between low vegetation surrounded by a square with parking lots and mid-rise buildings which enclose the square. Moreover, the station of Provinciehuis is located near a large four-story building that is situated in the west direction. The location in this broad urban canyon results in a SVF value of 0.59.

The **Plantentuin** station (LCZ 9) is positioned in the botanical garden of Ghent University, southwest from a large public park. Together they form a large green spot within the southern part of the city. The Plantentuin weather station is located in between trees and shrubs and the micro-environment of the station (10 m radius) consists of a complete pervious coverage. Due to the surrounding

trees the SVF (0.38) is relatively low. The completely green micro-environment of the Plantentuin stands in sharp contrast with the built-up features in the broader area around the station. At 565 m radius the impervious fraction increases to 65%.

Finally, the **Melle** location (LCZ D) is a rural place, characterised by a cover of low plants and it has a complete green coverage at a radius of 10 m. In contrast to the Plantentuin station, this station is placed above lawn in an open environment (SVF = 1.00). The wider environment around the station, at least up to 565 m, consist still out of a large proportion of green coverage (91%). The small impervious part is mainly due to the road segments but also some small groups of buildings occur.

A.5. Model statistics of UHI intensity summer 2016

The table below presents the average observed UHI intensity and model statistics (average UHI and RMSE with respect to observations) for summer (JAS) 2016. The statistics are calculated based on hourly values over the day period (defined from 5 UT till 19 UT) and night period (from 20 UT till 4 UT).

Daytime UHI					
	Average UHI (in °C)			Model RMSE (in °C)	
	MOCCA	UrbClim	ALARO-SURFEX	UrbClim	ALARO-SURFEX
Provinciehuis	0.96	0.83	0.57	1.04	1.18
Sint-Bavo	0.69	0.85	0.57	0.99	1.02
Honda	0.58	0.88	0.41	1.01	1.14
Plantentuin	−0.05	0.60	0.55	0.98	1.05
Wondelgem	0.36	0.60	0.53	1.01	1.14
Nighttime UHI					
	Average UHI (in °C)			Model RMSE (in °C)	
	MOCCA	UrbClim	ALARO-SURFEX	UrbClim	ALARO-SURFEX
Provinciehuis	2.18	2.77	2.11	1.51	1.47
Sint-Bavo	2.17	2.77	2.11	1.52	1.44
Honda	1.95	2.60	2.06	1.59	1.5
Plantentuin	1.38	1.85	1.5	1.34	1.33
Wondelgem	0.96	1.91	1.5	1.39	1.26

References

Agentschap Informatie Vlaanderen, “Bodembedekkingskaart (BBK), 1 m resolutie, opname 2012”, http://www.geopunt.be/catalogus/datasetfolder/b15fec52-6f04-4758-bef7-1b9063629aec, Dataset, published in 2016, consulted on 08/04/2018.

Arnfield, A.J., 2003. Two decades of urban climate research: a review of turbulence, exchanges of energy and water, and the urban heat island. Int. J. Climatol. 23, 1–26. https://doi.org/10.1002/joc.859.

Bassett, R., Cai, X., Chapman, L., Heaviside, C., Thornes, J., Muller, C., Duick, Y., Warren, E., 2016. Observations of urban heat island advection from a high-density monitoring network. Q. J. R. Meteorol. Soc. 142, 2434–2441. https://doi.org/10.1002/qj.2836.

Brandsma, T., Wolters, D., 2012. Measurement and statistical modeling of the urban Heat Island of the City of Utrecht (the Netherlands). J. Appl. Meteorol. Climatol. 51, 1046–1060. https://doi.org/10.1175/JAMC-D-11-0206.1.

Chapman, L., Muller, C., Young, D., Warren, E., Grimmond, C., Cai, X.M., Ferranti, E., 2015. The Birmingham urban climate laboratory. An open meteorological test bed and challenges of the Smart City. Bull. Am. Meteorol. Soc. 96, 1545–1560. https://doi.org/10.1175/BAMS-D-13-00193.1.

Danielson, J.J., Gesch, D.B., 2011. Global multi-resolution terrain elevation data 2010 (GMTED2010). In: U.S. Geological Survey Open-File Report, 2011 - 1073.

De Ridder, K., Schayes, G., 1997. The IAGL land surface model. J. Appl. Meteorol. Climatol. 36, 167–182. https://doi.org/10.1175/1520-0450(1997)036¡0167:TILSM¿2.0.CO;2.

De Ridder, K., Bertrand, C., Casanova, G., Lefebvre, W., 2012. Exploring a new method for the retrieval of urban thermophysical properties using thermal infrared remote sensing and deterministic modelling. J. Geophys. Res. 117, 2156–2202. https://doi.org/10.1029/2011JD017194.

De Ridder, K., Lauwaet, D., Maiheu, B., 2015. UrbClim - a fast urban boundary layer climate model. Urban Clim. 12, 21–48. https://doi.org/10.1016/j.uclim.2015.01.001.

Dee, D.P., Uppala, S.M., Simmons, A.J., Berrisford, P., Poli, P., Kobayashi, S., Andrae, U., Balmaseda, M.A., Balsamo, G., Bauer, P., Bechtold, P., Beljaars, A.C.M., van de Berg, L., Bidlot, J., Bormann, N., Delsol, C., Dragani, R., Fuentes, M., Geer, A.J., Haimberger, L., Healy, S.B., Hersbach, H., Hólm, E.V., Isaksen, L., Kållberg, P., Köhler, M., Matricardi, M., McNally, A.P., Monge-Sanz, B.M., Morcrette, J.J., Park, B.K., Peubey, C., de Rosnay, P., Tavolato, C., Thépaut, J.N., Vitart, F., 2011. The ERA-interim reanalysis: configuration and performance of the data assimilation system. Q. J. R. Meteorol. Soc. 137, 553–597. https://doi.org/10.1002/qj.828.

Ellefsen, R., 1990-1991. Mapping and measuring buildings in the urban canopy boundary layer in ten US cities. Energy Build. 15–16, 1025–1049.

García-Ddíez, M., Lauwaet, D., Hooyberghs, H., Ballester, J., De Ridder, K., Rodó, X., 2016. Advantages of using a fast urban boundary layer model as compared to a full mesoscale model to simulate the urban heat island of Barcelona. Geosci. Model Dev. 9, 4439–4450. https://doi.org/10.5194/gmd-9-4439-2016.

Gerard, L., 2007. An integrated package for subgrid convection, clouds and precipitation compati- ble with the meso-gamma scales. Q. J. R. Meteorol. Soc. 133, 711–730. https://doi.org/10.1002/qj.58.

Gerard, L., Geleyn, J.F., 2005. Evolution of a subgrid deep convection parametrization in a limited area model with increasing resolution. Q. J. R. Meteorol. Soc. 131, 2293–2312. https://doi.org/10.1256/qj.04.72.

Gerard, L., Piriou, J.M., Brožková, R., Geleyn, J.F., Banciu, D., 2009. Cloud and precipitation parameterization in a Meso-gamma-scale operational weather prediction model. Mon. Weather Rev. 137, 3960–3977. https://doi.org/10.1175/2009MWR2750.1.

Gutman, G., Ignatov, A., 1998. Derivation of green vegetation fraction from NOAA/AVHRR for use in weather prediction models. Int. J. Remote Sens. 19, 1533–1543.

Haeger-Eugensson, M., Holmer, B., 1999. Advection caused by the urban heat island circulation as a regulating factor on the nocturnal urban heat island. Int. J. Climatol. 19, 975–988. https://doi.org/10.1002/(SICI)1097-0088(199907)19:9¡975::AID-JOC399¿3.0.CO;2-J.

Hamdi, R., Masson, V., 2008. Inclusion of a drag approach in the Town Energy Balance (TEB) scheme: offline 1-D evaluation in a street canyon. J. Appl. Meteorol. Climatol. 47, 2627–2644. https://doi.org/10.1175/2008JAMC1865.1.
Hamdi, R., Van de Vyver, H., De Troch, R., Termonia, P., 2014. Assessment of three dynamical urban climate downscaling methods: Brussels's future urban heat island under an A1B emission scenario. Int. J. Climatol. 34, 978–999. https://doi.org/10.1002/joc.3734.
Hamdi, R., Giot, O., De Troch, R., Deckmyn, A., Termonia, P., 2015. Future climate of Brussels and Paris for the 2050s under the A1B scenario. Urban Clim. 12, 160–182. https://doi.org/10.1016/j.uclim.2015.03.003.
Hamdi, R., Duchêne, F., Berckmans, J., Delcloo, A., Vanpoucke, C., Termonia, P., 2016. Evolution of urban heat wave intensity for the Brussels Capital Region in the ARPEGE-Climat A1B scenario. Urban Clim. 17, 176–195. https://doi.org/10.1016/j.uclim.2016.08.001.
Kanda, M., Kanega, M., Kawai, T., Moriwaki, R., Sugawara, H., 2007. Roughness lengths for momentum and heat derived from outdoor urban-scale models. J. Appl. Meteorol. Climatol. 46, 1067–1079. https://doi.org/10.1175/JAM2500.1.
Koskinen, J., Poutiainen, J., Schultz, D., Joffre, S., Koistinen, J., Saltikoff, E., Gregow, E., Turtiainen, H., Dabberdt, W., Damski, J., Eresmaa, N., Göke, S., Hyvärinen, O., Järvi, L., Karppinen, A., Kotro, J., Kuitunen, T., Kukkonen, J., Kulmala, M., Moisseev, D., Nurmi, P., Pohjola, H., Pylkkö, P., Vesala, T., Viisanen, Y., 2011. The Helsinki Testbed: a Mesoscale measurement, research, and service platform. Bull. Am. Meteorol. Soc. 92, 325–342. https://doi.org/10.1175/2010BAMS2878.1.
Lauwaet, D., De Ridder, K., Saeed, S., Brisson, E., Chatterjee, F., van Lipzig, N.P.M., Maiheu, B., Hooyberghs, H., 2016. Assessing the current and future urban heat island of Brussels. Urban Clim. 15, 1–15. https://doi.org/10.1016/j.uclim.2015.11.008.
Lauwaet, D., Maiheu, B., De Ridder, K., Boënne, W., Hooyberghs, H., Demuzere, M., Verdonck, M.L., 2017. Effectiveness of Green and Blue Infrastructure to Mitigate Outdoor Heat Stress in the City of Ghent. Landscape and Urban Planning submitted, Belgium.
Lelovics, E., Unger, J., Gál, T., Gál, C.V., 2014. Design of an urban monitoring network based on local climate zone mapping and temperature pattern modelling. Clim. Res. 60, 51–62. https://doi.org/10.3354/cr012220.
Maiheu, B., Van den berghe, K., Boelens, L., De Ridder, K., Lauwaet, D., 2013. Opmaak van een hittekaart en analyse van het stedelijk hitte-eiland effect voor Gent. Dutch report on line available via. https://stad.gent/sites/default/files/page/documents/Hittestudie%20Gent.pdf.
Masson, V., 2000. A physically-based scheme for the urban energy budget in atmospheric models. Bound.-Layer Meteorol. 94, 357–397. https://doi.org/10.1023/A:1002463829265.
Masson, V., Seity, Y., 2009. Including atmospheric layers in vegetation and urban offline surface schemes. J. Appl. Meteorol. Climatol. 48, 1377–1397. https://doi.org/10.1175/2009JAMC1866.1.
Masson, V., Champeaux, J.L., Chauvin, F., Meriguet, C., Lacaze, R., 2003. A global database of land surface parameters at 1-km resolution in meteorological and climate models. J. Clim. 16, 1261–1282. https://doi.org/10.1175/1520-0442-16.9.1261.
Masson, V., Le Moigne, P., Martin, E., Faroux, S., Alias, A., Alkama, R., Belamari, S., Barbu, A., Boone, A., Bouyssel, F., Brousseau, P., Brun, E., Calvet, J.C., Carrer, D., Decharme, B., Delire, C., Donier, S., Essaouini, K., Gibelin, A.L., Giordani, H., Habets, F., Jidane, M., Kerdraon, G., Kourzeneva, E., Lafaysse, M., Lafont, S., Lebeaupin Brossier, C., Lemonsu, A., Mahfouf, J.F., Marguinaud, P., Mokhtari, M., Morin, S., Pigeon, G., Salgado, R., Seity, Y., Taillefer, F., Tanguy, G., Tulet, P., Vincendon, B., Vionnet, V., Voldoire, A., 2013. The SURFEXv7.2 land and ocean surface platform for coupled or offline simulation of earth surface variables and fluxes. Geosci. Model Dev. 4, 929–960. https://doi.org/10.5194/gmd-6-929-2013.
Matuschek, O., Matzarakis, A., 2010. Estimation of sky view factor in complex environment as a tool for applied climatological studies. Berichte des Meteorologischen Instituts der Albert-Ludwigs-Universität Freiburg 20, 534–539.
Matzarakis, A., Rutz, F., Mayer, H., 2010. Modelling radiation fluxes in simple and complex environments: basics of the RayMan model. Int. J. Biometeorol. 54, 131–139. https://doi.org/10.1007/s00484-009-0261-0.
Meier, F., Fenner, D., Grassmann, T., Otto, M., Scherer, D., 2017. Crowdsourcing air temperature from citizen weather stations for urban climate research. Urban Clim. 19https://doi.org/10.1016/j.uclim.2017.01.006. 170–19.
Misumi, R., Shoji, Y., Saito, K., Seko, H., Seino, N., Suzuki, S., Shusse, Y., Hirano, K., Belair, S., Chandrasekar, V., Lee, D.I., Filho, A.J.P., Nakatani, T., Maki, M., 2019. Results of the Tokyo Metropolitan Area Convection Study for extreme weather resilient cities (TOMACS). Bull. Am. Meteorol. Soc. 100, 2027–2041. https://doi.org/10.1175/BAMS-D-18-0316.1.
Muller, C.L., Chapman, L., Grimmond, C.S.B., Young, D.T., Cai, X., 2013. Sensors and the city: a review of urban meteorological networks. Int. J. Climatol. 33, 1585–1600. https://doi.org/10.1002/joc.3678.
Oke, T.R., 2004. Initial Guidance to Obtain Representative Meteorological Observations at Urban Sites. IOM Report No. 81 World Meteorological Organisation, Geneva.
Oke, T.R., 2006. Towards better scientific communication in urban climate. Theor. Appl. Climatol. 84, 179–190. https://doi.org/10.1007/s00704-005-0153-0.
Rotach, M.W., Vogt, R., Bernofer, C., Batchvarova, E., Christen, A., Clappier, A., Feddersen, B., Gryning, S.E., Martucci, G., Mayer, H., Mitev, V., Oke, T.R., Parlow, E., Richner, H., Roth, M., Roulet, Y.A., Ruffieux, D., Salmond, J.A., Schatsmann, M., Voogt, J.A., 2005. BUBBLE – an Ur-ban boundary layer meteorology project. Theor. Appl. Climatol. 81, 231–261. https://doi.org/10.1007/s00704-004-0117-9.
Royal Meteorological Institute of Belgium (RMI), 2019. Climate in Your Community. On line available via. http://www.meteo.be/meteo/view/nl/27484519-Klimaat+in+uw+gemeente.html.
Šećerov, I., Savić, S., Milošević, D., Marković, V., Bajšanski, D., 2015. Development of an automated urban climate monitoring system in Novi Sad (Serbia). Geographica Pannonica. 19, 174–183.
Skarbit, N., Stewart, I.D., Unger, J., Gál, T., 2017. Employing an urban meteorological network to monitor air temperature conditions in the 'local climate zones' of Szeged, Hungary. Int. J. Climatol. 37, 582–596. https://doi.org/10.1002/joc.5023.
Steeneveld, G.J., Koopmans, S., Heusinkveld, B.G., Theeuwes, N.E., 2014. Refreshing the role of open water surfaces on mitigating the maximum urban heat island effect. Landsc. Urban Plan. 121, 92–96. https://doi.org/10.1016/j.landurbplan.2013.09.001.
Stewart, I.D., 2011. A systematic review and scientific critique of methodology in modern urban heat island literature. Int. J. Climatol. 31, 200–217. https://doi.org/10.1002/joc.2141.
Stewart, I.D., Oke, T.R., 2012. Local climate zones for urban temperature studies. Bull. Am. Meteorol. Soc. 93, 1879–1900. https://doi.org/10.1175/BAMS-D-11-00019.1.
Stewart, I.D., Oke, T.R., Krayenhoff, E.S., 2014. Evaluation of the "local climate zone" scheme using temperature observations and model simulations. Int. J. Climatol. 34, 1062–1080. https://doi.org/10.1002/joc.3746.
Termonia, P., Fischer, C., Bazile, E., Bouyssell, F., Brožková, R., Bénard, P., Bochenek, B., Degrauwe, D., Derkova, M., El Khatib, R., Hamdi, R., Mašek, J., Pottier, P., Pristov, N., Seity, Y., Smolíková, P., Spaniel, O., Tudor, M., Wang, Y., Wittmann, C., Joly, A., 2018. The ALADIN System and its Canonical Model Configurations AROME CY41T1 and ALARO CY40T1. Geosci. Model Dev. 11, 257–281. https://doi.org/10.5194/gmd-11-257-2018.
Theeuwes, N.E., Solcerova, A., Steeneveld, G.J., 2013. Modelling the influence of open water surfaces on the summertime temperature and thermal comfort in the city. J. Geophys. Res. Atmos. 118, 8881–8896. https://doi.org/10.1002/jgrd.50704.
Theurer, W., 1999. Typical building arrangement for urban air pollution modelling. Atmos. Environ. 33, 4057–4066. https://doi.org/10.1016/S1352-2310(99)00147-8.
Van Hove, L.W.A., Jacobs, C.M.J., Heusinkveld, B.G., Elbers, J.A., Van Driel, B.L., Holtslag, A.A.M., 2015. Temporal and spatial variability of urban heat island and thermal comfort within the Rotterdam agglomeration. Build. Environ. 83, 91–103. https://doi.org/10.1016/j.buildenv.2014.08.029.
Vandemeulebroucke, I., Calle, K., Caluwaerts, S., De Kock, T., Van Den Bossche, N., 2019. Does historic construction suffer or benefit from the urban heat island effect in Ghent and global warming across Europe? Can. J. Civ. Eng. 46, 1032–1042. https://doi.org/10.1139/cjce-2018-0594.
Verdonck, M.L., Okujeni, A., van der Linden, S., Demuzere, M., De Wulf, R., Van Coillie, F., 2017. Influence of neighbourhood information on 'Local Climate Zone' mapping in heterogeneous cities. Int. J. Appl. Earth Obs. Geoinf. 62, 102–113. doi.org/10.1016/j.jag.2017.05.017.
Wang, Y., Bakker, F., de Groot, R., Wortche, H., Leemans, R., 2015. Effects of urban trees on local outdoor microclimate: synthesizing field measurements by numerical modelling. Urban Ecosyst. 18, 1305–1331. https://doi.org/10.1007/s11252-015-0447-7.
White, R., Engelen, G., Uljee, I., 2015. Modeling Cities and Regions as Complex Systems. The MIT press, Cambridge, MA 02142, USA, pp. 330.
WMO, 2008. Guide to Meteorological Instruments and Methods of Observation. In: Instruments and Observing Methods Report No. 8.